Alternatively spliced domains interact to regulate BK potassium channel gating

Brandon E. Johnson[a], Dominique A. Glauser[a,1], Elise S. Dan-Glauser[b], D. Brent Halling[c], Richard W. Aldrich[c,2], and Miriam B. Goodman[a,2]

[a]Department of Molecular and Cellular Physiology, Stanford University, Stanford, CA 94305; [b]Department of Psychology, Stanford University, Stanford, CA 94305; and [c]Section of Neurobiology, Center for Learning and Memory, University of Texas, Austin, TX 78712

Contributed by Richard W. Aldrich, October 12, 2011 (sent for review June 19, 2011)

Most human genes contain multiple alternative splice sites believed to extend the complexity and diversity of the proteome. However, little is known about how interactions among alternative exons regulate protein function. We used the *Caenorhabditis elegans slo-1* large-conductance calcium and voltage-activated potassium (BK) channel gene, which contains three alternative splice sites (A, B, and C) and encodes at least 12 splice variants, to investigate the functional consequences of alternative splicing. These splice sites enable the insertion of exons encoding part of the regulator of K^+ conductance (RCK)1 Ca^{2+} coordination domain (exons A1 and A2) and portions of the RCK1–RCK2 linker (exons B0, B1, B2, C0, and C1). Exons A1 and A2 are used in a mutually exclusive manner and are 67% identical. The other exons can extend the RCK1–RCK2 linker by up to 41 residues. Electrophysiological recordings of all isoforms show that the A1 and A2 exons regulate activation kinetics and Ca^{2+} sensitivity, but only if alternate exons are inserted at site B or C. Thus, RCK1 interacts with the RCK1–RCK2 linker, and the effect of exon variation on gating depends on the combination of alternate exons present in each isoform.

Slo1 channels | regulator of K conductance domains | *C. elegans*

Alternative splicing is observed in all eukaryotic organisms and diversifies the proteome encoded by metazoan genomes while preserving their compact sizes. Most human genes (90%) encode multiple transcripts (1, 2), and on average, each multiexon gene encodes at least seven distinct transcripts (1). Although alternative splicing is known to change protein function by adding, removing, or altering functional domains (3, 4), the combinatorial effects of alternative splicing across multiple sites on protein function have not been examined previously. To address these questions, we examined the functional differences among isoforms of the *slo1* gene that is conserved among metazoans and subject to extensive alternative splicing (5, 6). The *slo1* gene in *Drosophila* and its ortholog in humans, *KCNMA1*, encode 10 and 13 alternate exons, respectively (5). If all possible exon combinations were to be expressed, then each of these genes would encode more than 1,000 transcripts. By contrast, the *Caenorhabditis elegans slo-1* gene is much simpler, with three alternate splice sites (7) and 12 possible splice variants. Thus, the *C. elegans slo-1* gene offers an opportunity for a comprehensive analysis of the functional diversity of splice variants generated by a single gene that is conserved from worms to humans.

slo1 encodes the pore-forming subunit of large-conductance, Ca^{2+}- and voltage-activated K^+ (BK) channels. Accordingly, functional changes caused by alternative splicing are readily measured using the patch-clamp technique. BK channels regulate cellular excitability by linking Ca^{2+} signaling to membrane repolarization and are essential for vascular tone (8–10), endocrine secretion (11, 12), neurotransmitter release (13, 14), and frequency tuning in hair cells (15). BK channel isoforms are adapted to function in specific cell types, developmental stages, or during physiological stress (16–21).

BK channels are tetrameric complexes with a central conducting pore, a voltage-sensing domain, and a cytosolic Ca^{2+}-coordination domain. The cytosolic domain is the locus of a majority of alternate splice sites (6) and harbors two high-affinity Ca^{2+}-sensitive regulator of K^+ conductance (RCK) domains (22–24). Crystal structures solved for the cytoplasmic domain of the human BK channel in the presence (25) and absence (26) of Ca^{2+} show that each BK channel subunit coordinates tandem RCK domains that assemble into a gating ring. A cryo-EM structure of the human BK channel indicates that the gating ring is positioned directly below the transmembrane pore (27).

Both RCK domains are important for Ca^{2+}-dependent activation, and the second RCK domain contains an aspartate-rich Ca^{2+} bowl likely to coordinate Ca^{2+} (23). RCK domains from adjacent subunits stabilize the assembly of the gating ring in a tetrameric arrangement (25, 26, 28), and the apparent BK channel Ca^{2+} coordination site resides near the assembly interface (25, 26). The BK channel RCK domains are connected by an RCK1–RCK2 linker, whose sequence is poorly conserved between species, and has yet to be resolved in crystal structures. However, functional studies highlight its significance by showing that alternative splicing (29), phosphorylation (30), and heme coordination (31) in this region can modify channel function.

Nematode and insect *slo1* genes contain alternative exons that encode and diversify the amino acid sequence of the C-terminal end of RCK1 and the RCK1–RCK2 linker (6). The *slo1* gene in nematodes and insects encodes a pair of paralogous cassette exons that are mutually exclusive (6) and encode 37 residues that align with the C-terminal subdomain of RCK1. These paralogs could potentially modulate Ca^{2+}-dependent gating by virtue of their proximity to the Ca^{2+} bowl in RCK2 (25, 26). Alternative splicing in the RCK1–RCK2 linker also affects the apparent Ca^{2+} sensitivity of the channel (29, 32).

In this study, we determine how alternative splicing of the *C. elegans slo-1* gene affects BK channel function. Like native BK channels in other organisms, heterologously expressed *C. elegans* BK channel isoforms display variable activation rates and apparent Ca^{2+} sensitivities but have similar voltage dependences. A majority of the phenotypic variation among isoforms is caused by the identity of the paralogous alternative exon encoding a portion of RCK1. However, the impact of this exon on BK channel function depends on which exon is inserted at the two other alternative splice sites in the RCK1–RCK2 linker. Thus, combinatorial variations at all three sites have a strong effect on function, and interactions between RCK1 and the RCK1–RCK2 linker modulate Ca^{2+}-dependence of channel activation.

Author contributions: B.E.J., R.W.A., and M.B.G. designed research; B.E.J. performed research; B.E.J., D.A.G., E.S.D.-G., D.B.H., and M.B.G. analyzed data; and B.E.J., D.A.G., E.S.D.-G., D.B.H., R.W.A., and M.B.G. wrote the paper.

The authors declare no conflict of interest.

[1]Present address: Department of Biology/Zoology, University of Fribourg, 1700 Fribourg, Switzerland.

[2]To whom correspondence may be addressed. E-mail: raldrich@mail.utexas.edu or mbgoodman@stanford.edu.

This article contains supporting information online at www.pnas.org/lookup/suppl/doi:10.1073/pnas.1116795108/-/DCSupplemental.

Results

The *slo1* gene encodes multiple transcripts in all metazoans from nematodes to vertebrates (5, 6). Three splice variants have been reported previously in *C. elegans*: SLO-1a, SLO-1b, and SLO-1c (7). These three transcripts demonstrate that the *C. elegans slo-1* gene has at least three alternate splice sites and that it is the target of a variety of splicing events, including the mutually exclusive insertion of paralogous cassette exons and exon skipping. To simplify the discussion of *slo-1* transcripts and the proteins they encode, we introduce a nomenclature similar to that used to describe alternative splicing in *Drosophila slo1* (32). In this system (Table S1), each alternative splice site is assigned an uppercase letter, and each exon is assigned a numerical value (a value of zero indicates that the exon is skipped). As illustrated in Fig. 1 and Table S2, site A inserts one of two mutually exclusive exons: A1 or A2. Site B either skips exon 13 (B0) or inserts one of two exons with alternate 5′ acceptor sites: B1 or B2. At site C, exon 15 is either skipped (C0) or inserted (C1).

To determine whether all 12 predicted *slo-1* splice variants are expressed, we combined the ability of RT-PCR to detect transcripts expressed at low levels with the specificity of restriction enzymes to identify the exons present in the pool of amplified cDNA molecules (*SI Materials and Methods*). We applied this strategy to total RNA from mixed populations of *C. elegans* that span all developmental stages to discover *slo-1* transcripts that may be expressed only in embryos, larvae, or adults. We detected and cloned the variable region of all 12 predicted transcripts, resulting from all possible combinations of alternative splicing at sites A, B, and C (*Materials and Methods*): the three known transcripts plus nine previously unreported ones.

SLO-1 Variants Form Voltage- and Ca^{2+}-Dependent K^+ Channels in *Xenopus* Oocytes. All *C. elegans* SLO-1 proteins form functional channels with qualitatively similar macroscopic activation kinetics when expressed in *Xenopus* oocytes (Fig. 2). Fig. S1 shows a detailed characterization of SLO-1(A2;B0;C1), previously named SLO-1a. Similar to SLO-1(A2;B0;C1), all channel isoforms reach steady-state current levels within 10 ms (in 5 μM Ca^{2+}), do not inactivate over 10 ms, and deactivate very rapidly (τ <0.5 ms). The only discernable kinetic difference between isoforms is a variation in activation rate (Fig. 2). The identity of the exon inserted at splice site A may account for these kinetic differences because A1-type variants activate faster than A2-type (Fig. 2*B*). We tested this inference using two-way ANOVAs for all six splice variant pairs that differ only at site A. This analysis considers measurements taken across the entire voltage range and reveals that activation rates for five of the six splice variant pairs are significantly different [$F_{(1,51–72)}$ = 15.54–114.07, P < 0.001]. There was no significant effect of the identity of the A exon in one pair: A1;B1;C1 and A2;B1;C1 [$F_{(1,54)}$ = 0.82, P = 0.37].

Alternative splicing in the BK channel C-terminal domain tunes voltage and Ca^{2+} sensitivity of fly and vertebrate BK channels (16, 29, 33). To determine whether alternative splicing in *C. elegans slo-1* confers similar functional variability in *C. elegans* BK channels, we determined *G–V* curves for all splice variants over a wide range of Ca^{2+} concentrations and voltages (Fig. S2). Alternative splicing does not directly modulate apparent voltage sensitivity,

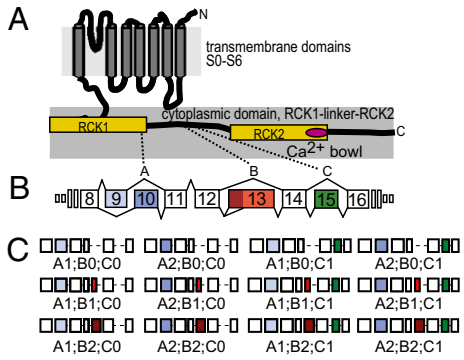

Fig. 1. *C. elegans slo-1* splice variants. (*A*) Schematic topology diagram of SLO-1 protein showing seven transmembrane domains (S0–S6), two calcium-sensitive domains (RCK1 and RCK2, yellow), and the Ca^{2+} bowl (magenta). (*B*) *C. elegans slo-1* gene structure. Each alternate splice site was assigned a letter (A, B, or C), and each alternative exon was assigned a number; zero indicates skipped exons. Splice site A regulates the insertion of two mutually exclusive exons (exons 9 and 10). Transcripts with exon 9 are indicated by "A1" and those with exon 10 are indicated by "A2". Splice site B is spliced in three ways: a type I deletion (exon 13 skipped, B0), a newly discovered type II deletion (5′ truncation of exon 13, B1), and incorporation of the full-length exon 13 (B2). Splice site C is a type I splice site where exon 15 is either skipped (C0) or inserted (C1). Boxes indicate constitutive (open) and alternate (filled) exons, lines show introns (not to scale). Alternate exons encode part of the RCK1 domain and two regions in the RCK1–RCK2 linker. (*C*) Schematic of all possible exon combinations between exon 8 and 16.

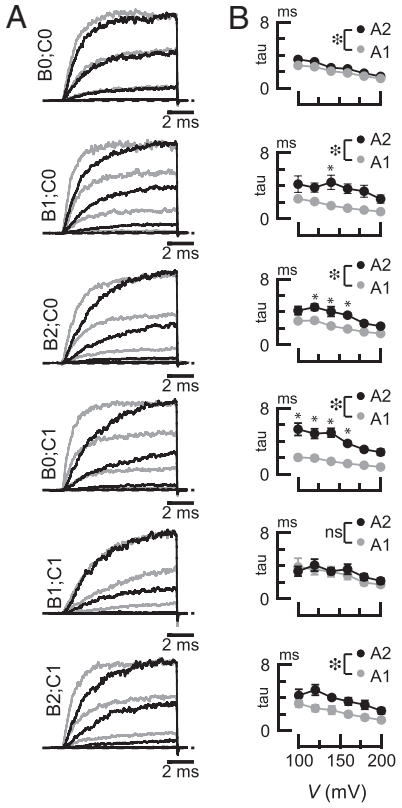

Fig. 2. Effects of alternative splicing on BK channel activation kinetics. (*A*) Average macroscopic currents evoked by 10-ms voltage steps from a −80 mV holding potential splice variants exposed to 5 μM Ca^{2+}. Zero current is shown by the dashed line; light and dark traces are for A1- and A2-type variants, respectively. For clarity, only three traces are shown. Similar results were obtained for at least five patches per isoform. (*B*) Mean activation time constants for the splice variants shown in *A*. Open circles are A1-type variants, and filled circles are A2-type variants. Each point is the mean ± SEM (n ≥ 5). Differences between splice variant pairs were evaluated across the full voltage range by two-way ANOVAs and Bonferroni post hoc tests. Large asterisks (✻) indicate significant main effect of the A exon variant by ANOVA (P < 0.001). *Significant differences (P < 0.01) between pairs of measurements at a single voltage by Bonferroni post hoc tests. ns, not significant (P > 0.01). F statistics and P values for ANOVAs were (*Top* to *Bottom*): $F_{(1,72)}$ = 15.54, P < 0.001; $F_{(1,51)}$ = 43.02, P < 0.001; $F_{(1,54)}$ = 50.47, P < 0.001; $F_{(1,60)}$ = 114.07, P < 0.001; $F_{(1,54)}$ = 0.82, P = 0.37; and $F_{(1,66)}$ = 25.07, P < 0.001.

because the equivalent gating charge (z) was not significantly different across splice variants tested at 5 μM $[Ca^{2+}]_i$ ($\langle z \rangle$ = 1.18 ± 0.13, minimum 1.07, maximum 1.29). Alternative splicing does modulate apparent Ca^{2+} sensitivity, however. As found for other BK channels, $V_{1/2}$ decreases as $[Ca^{2+}]_i$ increases (Fig. S2*B*). Across the entire range of Ca^{2+} concentrations examined (2–300 μM), A1-type variants activated at more negative voltages than the corresponding A2-type variants [main effect of A-variants by two-way ANOVAs, $F_{(1,61–80)}$ = 15.06–127.38, $P < 0.001$]. The only exception is the A1;B0;C0 and A2;B0;C0 pair, which have indistinguishable Ca^{2+} dependence [$F_{(1,84)} = 5.03$, $P = 0.03$].

Does Alternative Splicing at an Individual Splice Site Account for Variation Among Isoforms? We grouped splice variants by exon composition and compared how alternative splicing at each site affects activation kinetics (Fig. 3 *A–C*) and gating (Fig. 3 *D–F*). Across the full voltage range, the six A1-type variants activate faster, on average, than the six A2-type variants [$F_{(1,417)} = 178.08$, $P < 0.01$ (Fig. 3*A*)]. Analysis of exon insertion at site B [$F_{(2,411)} = 5.16$, $P < 0.01$ (Fig. 3*B*)] and C [$F_{(1,417} = 16.52$, $P < 0.01$ (Fig. 3*C*)] indicated slower activation in B2 variants compared with B0 variants, as well as slower activation in C1 variants compared with C0 variants. However, effect sizes for B and C types were much smaller than for A types. Thus, alternative splicing at site A has the biggest impact on activation kinetics.

The effect of alternative splicing on apparent voltage dependence (Fig. 3 *D–F*) could reflect differences in apparent Ca^{2+} sensitivity or in the Ca^{2+} independent free energy required to shift channels from the closed to the open conformation. The change in free energy is given by: $\Delta G = -zeV_{1/2}$, where z and $V_{1/2}$ values are obtained by fitting $G–V$ curves with a Boltzmann function, and e is the elementary charge of an electron (34). To determine how alternative splicing affects gating energy, we plotted $zV_{1/2}$ as a function of Ca^{2+} for all splice variants (Fig. 3 *D–F*) and assessed differences with two-way ANOVAs. We found that ΔG was lower for A1-type variants than for A2-type variants [$F_{(1,488)} = 128.20$, $P < 0.01$]. This effect was most prominent at Ca^{2+} concentrations below 20 μM (Fig. 3*D*). The same analysis applied to B-type exons showed an effect of alternative splicing at site B [$F_{(2,481)} = 6.25$, $P < 0.01$]. ΔG is lower for B0-type variants than B1-type ($P < 0.01$, by Bonferonni post hoc test; Fig. 4*E*). The same approach highlighted no overall difference between C0-type and C1-type splice variants [$F_{(1,417)} = 16.52$, P = not significant] (Fig. 3*F*).

Seven Alternate Exons in *slo-1* Regulate BK Channel Gating in Concert. Our analysis of splice variants pooled according to exon choice at sites A, B, or C (Fig. 3) shows the average contribution of specific exons to activation kinetics and steady-state activation of the channel. However, these general trends are not observed in all isoforms. For example, the impact of exon choice at site A on τ and $V_{1/2}$ depends on the exons inserted at sites B and C (compare A1 and A2 in Fig. 2*B* and Fig. S2*B*). To address the putative functional interaction between alternative exons in more details, we undertook a comprehensive analysis to track the effects of splicing at all three sites. We used a multifactorial ANOVA with three factors (exon identity at site A, site B, and site C) and analyzed how they affect $zV_{1/2}$ values at 5 μM Ca^{2+}. Consistent with the splice variant pool analysis (Fig. 3 *D–F*), the ANOVA revealed main effects of A-type [$F_{(2,60)} = 98.5$, $P < 0.01$] and B-type exons [$F_{(2,60)} = 9.8$, $P < 0.01$], but no main effect of C-type exons [$F_{(2,60)} = 0.4$, $P = 0.55$] on $zV_{1/2}$. In addition, a significant triple interaction effect (A × B × C) was found [$F_{(2,60)} = 6.1$, $P < 0.01$], confirming a complex interplay between exons at all three sites in governing channel gating.

Using Tukey post hoc tests after the multifactorial ANOVA, we compared $zV_{1/2}$ values for all splice variants pairs (66 total comparisons) and identified significant differences among ≈35% (23 of 66) of all splice variant pairs (Table S3). Much of this variation in gating energy seems to be conferred by the A-type exons. Indeed,

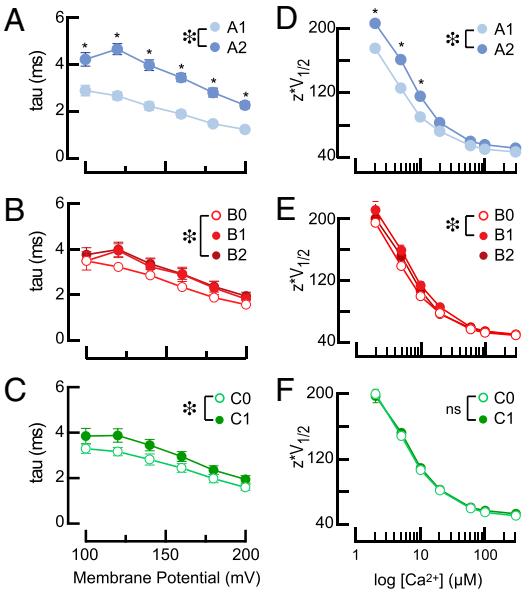

Fig. 3. Effects of variations at single splice sites on activation kinetics (τ, *A–C*) and $zV_{1/2}$ (*D–F*). (*A–C*) Activation time constants (at 5 μM Ca^{2+}) as a function of exon type. (*A*) A1-type (n = 35) and A2-type (n = 37) splice variants. (*B*) B0-type (n = 26), B1-type (n = 22), and B2-type (n = 24) splice variants. (*C*) C0-type (n = 37) and C1-type (n = 37) splice variants. (*D–F*) Mean $zV_{1/2}$ as a function of exon type. (*D*) A1-type (n = 35) and A2-type (n = 37). (*E*) B0-type (n = 26), B1-type (n = 22), and B2-type (n = 24). (*F*) C0-type (n = 37) and C1-type (n = 37). All points are mean ± SEM; error bars are smaller than symbols in some cases. The effect of exon type was evaluated across the full voltage range (*A–C*) or Ca^{2+} concentration range (*D–F*) by two-way ANOVAs and Bonferroni post hoc tests. Large asterisks (✻) indicate significant main effect of exon A variant by ANOVA: (*A*) $F_{(1,417)} = 178.08$, $P < 0.01$; (*B*) $F_{(2,411)} = 5.16$, $P < 0.01$; (*C*) $F_{(1,417)} = 16.52$, $P < 0.01$; (*D*) $F_{(1,488)} = 128.20$, $P < 0.01$; (*E*) $F_{(2,481)} = 6.25$, $P < 0.01$. *Significant differences ($P < 0.01$) at individual voltages (A–C) or Ca^{2+} concentrations (*D–F*) by Bonferroni post hoc tests.

of the 23 pairs of splice variants that are functionally distinct, 21 have different exons inserted at site A (A1 vs. A2). The functional differences between A1- and A2-type variants is evident only when either splice sites B or C contains an exon because no significant difference in $zV_{1/2}$ was detected between the SLO-1(A1;B0;C0) and SLO-1(A2;B0;C0) isoforms. These results suggest that the impact produced by the alternate exon inserted at site A on channel gating is modulated by the protein context at sites B and C.

To learn more, we evaluated the impact of alternate splicing on channel gating energetics. If variations at individual splice sites cannot fully account for the functional differences between splice variants, then variations at site A would not show similar energetic differences in all B- and C-type backgrounds. We addressed this hypothesis by calculating the difference in free energy conferred by converting an A1-type variant to an A2-type variant: $\Delta\Delta G = \Delta G_{A1;BX;CY} - \Delta G_{A2;BX;CY}$, where the subscript indicates the splice variant, B*X* is the identity of the exon inserted at site B, and C*Y* is the exon inserted at site C (Fig. 4*A*). As expected from the analysis presented in Table S3, the energetic difference between an A1- and an A2-type variant is small and not significantly different in a B0;C0 background. Inserting either B1 or B2 significantly enhances the energetic difference conferred by replacing A1 with A2. Thus, variations at splice site B can enhance the energetic differences caused by a variation at site A. To determine how variations at site C affect the functional interactions between sites A and B, we made a similar energetic comparison in a C1 background. Replacing C0 with C1 increases the free energy change associated with replacing A1 with A2. This maneuver also eliminates the differences associated with alternative splicing at

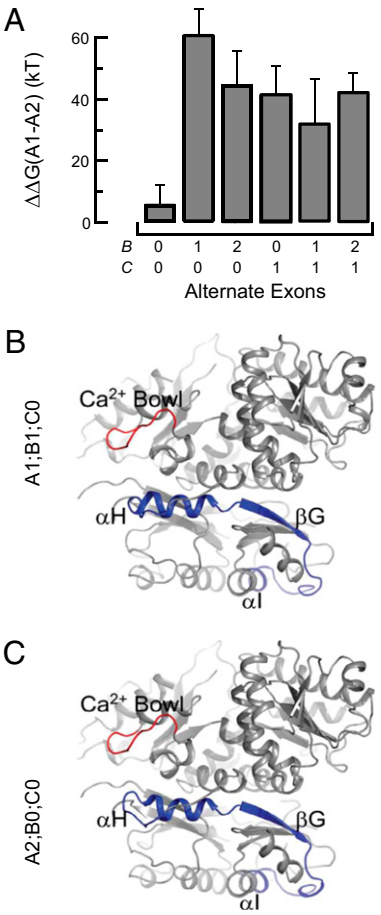

Fig. 4. Replacing A1 with A2 changes gating energies and a portion of RCK1. (*A*) Change in free energy, $\Delta\Delta G$, conferred by replacing A1 with A2. Each bar was computed from $zV_{1/2}$ for the A1-type and A2-type splice variants with the indicated composition at sites B and C. Errors were propagated from the SD of $zV_{1/2}$ in the relevant A1-type and A2-type splice variants. (*B*) SLO-1(A1;B1;C0) homology model threaded to the human BK channel cytoplasmic domain crystal structure (3MT5). RCK domains are shown in gray, the Ca^{2+} bowl is red, and the region encoded by A1 (α-H, β-G, and α-I) is shown in blue. (*C*) Same as in *B*, except showing SLO-1(A2;B0;C0) with the region encoded by A2 shown in blue.

site B in the C0 background. These results demonstrate that alternate exons in the *C. elegans slo-1* gene act in concert to regulate the free energy change associated with gating.

Alternatively Spliced αH Helix of RCK1 Is Close to the Calcium Bowl in RCK2. Because alternative splicing at site A regulates activation kinetics and Ca^{2+}-dependent activation and alters the sequence of the C-terminal subdomain of RCK1, we sought to discover potential interactions between this region and other portions of the BK channel. Toward this end, we derived 3D models of the cytoplasmic domain of SLO-1(A2;B0;C0) and SLO-1(A1;B1;C0) from the available crystal structures of the human BK channel cytosolic domain (25, 26). From the crystal structures, the C-terminal end of RCK1 that corresponds to site A (both A1 and A2 are 41% identical to the human sequence) includes two α-helices and a β-sheet: αH, βG, and αI. We found that the αH helix is in close proximity to the Ca^{2+}-bowl (Fig. 4 *B* and *C*). Indeed, the backbone carbons of αH and the Ca^{2+}-bowl are within 12 Å of one another, consistent with the idea that these two subdomains could come close enough to interact with a small change in protein conformation. Alternative splicing at site A may thus change the chemical environment of the calcium bowl region and could directly affect the Ca^{2+}-binding affinity or the conformational changes executed by the gating ring upon Ca^{2+} binding.

Discussion

In *C. elegans*, as in mammals, BK channels are widely expressed in both nerve and muscle (7, 35) and regulate excitability in both tissues (7, 36, 37). Whereas slo-1 mutants establish the importance of BK channels for *C. elegans* physiology, they provide little insight into the contribution of alternative splicing. We show that SLO-1 splice variants differ in their apparent Ca^{2+} sensitivity and kinetics and propose that the range of biophysical properties generated by alternative splicing is essential for physiology. Two findings support this inference. First, prior work shows that a change in voltage-dependence of 40 mV is sufficient to alter behavior and decrease synaptic transmission (35). A similiar shift in voltage-dependence would arise if SLO-1(A1;B0;C1) were expressed instead of SLO-1(A2;B1;C0). Second, we show in a companion paper (38) that a mutation that alters the distribution of splice variants, but has no effect on coding sequence, increases aldicarb sensitivity, an effect which is consistent with a reduction in BK channel function.

Functional Variation Among Splice Variants Reveals Interaction Between Alternate Exons. By contrast with purely voltage-gated ion channels, which achieve diversity by virtue of being encoded by large gene families, the BK channel pore-forming subunit is encoded by a single gene that contains a multitude of alternative splice sites, suggesting that alternative splicing diversifies the functional properties of BK channels within and among tissues (30, 39–41). The number of identified *slo1* transcripts in *Drosophila* and vertebrates represent a small fraction of the more than 1,000 splice variants predicted from the gene sequences, but *C. elegans slo-1* has provided an opportunity to examine how alternative splicing across multiple splice sites diversifies BK channel function.

Here, we show that 12 predicted *C. elegans slo-1* transcripts are expressed in vivo and form functional channels in heterologous cells, demonstrating that all splice variants encode fully functional channels. Alternative splicing of the RCK1 domain and the RCK1–RCK2 linker of *C. elegans* BK channels affects activation kinetics and apparent Ca^{2+} sensitivity but does not have a detectable effect on voltage sensitivity in channels expressed in *Xenopus* oocytes. No single alternate exon substitution can account for all variations in BK channel kinetics or in the apparent Ca^{2+} sensitivity of gating. Rather, interactions among alternate exons give rise to the functional profile that is characteristic of each splice variant. If *slo1* genes in other species are similar, then these results indicate that alternative splicing of *slo1* is likely to produce a rich palette of hundreds or even thousands of BK channel isoforms with distinct functional properties. The potential for heterotetrameric channels is another factor that could extend this palette even further.

RCK1–RCK2 Linker Functionally Interacts with the RCK1 Domain. The A1 and A2 exons in *C. elegans slo-1* encode the C-terminal subdomain of RCK1 (αH, βG, and αI), whereas the B-type and C-type exons encode portions of the RCK1–RCK2 linker. Crystal structures of the human BK channel C-terminal domain have provided invaluable insight into how the RCK domains fold into the structural configuration of the gating ring. One study suggests that Ca^{2+} is coordinated by the Ca^{2+}-bowl at the interface between the RCK1 and RCK2 domains of adjacent subunits in the tetrameric complex (25). Point mutations in the RCK1 domain can decrease or enhance Ca^{2+} sensitivity (22, 42, 43), and our results show that altering the C-terminal portion of the RCK1 domain can also change Ca^{2+} sensitivity. In particular, A1-type splice variants activate at lower voltages and Ca^{2+} concentrations than A2-type splice variants.

The RCK1–RCK2 linker was not resolved in the structures of either Ca^{2+}-bound or Ca^{2+}-free BK channel cytoplasmic domains

PHYSIOLOGY

(25, 26). Prior work has suggested that the specific amino acid sequence of this region is unimportant as long as it is long enough to connect RCK1 to RCK2 (25, 44). The present work establishes a functional interaction between the RCK1–RCK2 linker and the C-terminal domain of RCK1, which affects the Ca^{2+} dependence of channel activation. The impact of alternative splicing on channel function could reflect a physical interaction between RCK1 and the RCK1–RCK2 linker, or impose a more global structural change. Additional structural information is needed to resolve this question and to assess how alternative splicing affects the structure of the RCK1–RCK2 linker.

The biophysical properties of A1-type and A2-type isoforms are indistinguishable if, and only if, the alternate exons at sites B and C are skipped to form a minimal RCK1–RCK2 linker. We propose that this linker is long enough to connect RCK1 to RCK2 but lacks the ability to modify the potential interaction between RCK1 and the calcium bowl that can fine-tune both activation kinetics and Ca^{2+} dependence. The insertion of alternate exons at sites B and C lengthens the RCK1–RCK2 linker and reveals functional differences between the A1-type and A2-type isoforms. For example, the Ca^{2+} sensitivity of SLO-1(A1;B0;C0) and SLO-1(A2;B0;C0) are indistinguishable, whereas SLO-1(A1;B1;C0) activates at lower Ca^{2+} concentrations than SLO-1(A2;B1;C0). Thus, exon B1 potentiates an interaction between the C-terminal subdomain of RCK1 and the Ca^{2+}-dependent gating mechanism that is not possible when no exon is inserted at site B. Although the structural basis for this interaction is unknown, we demonstrate that naturally occurring variations in the RCK1–RCK2 linker profoundly affect BK channel gating.

We have shown that alternate exons fine-tune BK channel activation kinetics and energy in a coordinated manner and that the splicing events responsible for generating BK channel isoforms are likewise coordinated and interdependent (38). It is likely that this coordinate, interactive splicing strategy is not unique to *slo-1*. Thus, whereas some genes use alternate splicing to regulate functionally independent modules, we propose that some other genes (like *slo-1*) use alternate splicing to coordinate functionally interacting modules and that still other genes may use a combination of these strategies.

Materials and Methods

SI Materials and Methods contains details of splice variant identification, plasmids, and methods for *Xenopus* oocyte expression of *C. elegans* SLO-1 BK channel isoforms.

Electrophysiological Recording Solutions. External recording solutions consisted of: $KMeSO_4$ (140 mM), KCl (6 mM), and KHepes (20 mM), pH 7.2. Solutions of defined Ca^{2+} concentrations were made by adding $CaCl_2$ (0.1 mM) and the following Ca^{2+} buffers: nitriloacetic acid (5 mM) for 50–60 μM Ca^{2+}; HEDTA (5 mM) for 3–20 μM Ca^{2+}; and EGTA (5 mM) for 2 μM Ca^{2+} solution. Free Ca^{2+} concentration was measured using an Orion ionplus 9320BN Ca^{2+} electrode (Thermo Fisher Scientific) attached to a phi-350 pH meter (Beckman Coulter). The Ca^{2+} electrode was calibrated by adding a serial dilution of 0.1 M $CaCl_2$ (Thermo Fisher Scientific) to non-Ca^{2+} buffered external recording solution. The pipette solution consisted of: $KMeSO_4$ (140 mM), KCl (6 mM), $MgCl_2$ (2 mM), and KHepes (20 mM), pH 7.2. Recording electrodes were pulled from borosilicate glass (BF150-110-10; Sutter Instruments), coated with wax (Kerrlab), and pressure polished (45). When filled with recording solutions, electrode resistances were between 0.7 and 1.5 MΩ.

Patch Clamp Electrophysiology. Currents were measured in inside-out patches with symmetric K^+ concentrations using a patch clamp amplifier [WPC-100 (Bioscience Tools) or EPC-10 (HEKA)]. To determine the voltage dependence of channel gating, we applied a series of voltage pulses (5–30 ms in duration) from a holding potential of −80 mV to a potential of 200 mV (in 10-mV increments). We matched the voltage pulse durations to the amount of time required for currents to reach and hold a steady-state value for at least 1 ms. Calcium sensitivity was determined by exposing excised patches to a series of buffered Ca^{2+} solutions, using a 16-channel microfluidic chip (Cellectricon). Maximum patch currents were 2–6.5 nA in amplitude. Analog data were filtered at 10 kHz and sampled at 100 kHz, using an eight-pole Bessel filter (FLA-01; Cygnus Technology) and HEKA Patchmaster v2.15 software. Conductance (G) was derived from steady-state currents according to Ohm's law ($G = I/(V - E_K)$, where $E_K = 0$ mV because the K^+ ion concentration is the same on both sides of the patch) and used to derive the G–V relationship for each patch. All voltages were corrected for series resistance offline, which we estimated to be twice the pipette resistance (2 MΩ). The differences in $V_{1/2}$ values between noncorrected and corrected voltages were less than 2 mV. G–V curves were fit by the Boltzmann equation $G/G_{max} = 1/1 + \exp((V - V_{1/2})zF/RT)$, where $V_{1/2}$ is the voltage of half-maximum conductance, z is the slope of the curve, and R, T, and F have the usual meaning. All electrophysiology data were collected at 22 ± 1 °C.

Homology Modeling. Structures of the RCK domains from human BK channel were solved previously (25, 26). The Web-based homology modeler ModWeb was used to thread the sequence of the worm BK channel onto the human BK crystal structures (46). Figures for the models were prepared using The PyMOL Molecular Graphics System (version 0.99; Schrödinger). Residues of the worm BK channel that align with residues that are disordered or absent in the human BK crystal structure were omitted from the figure.

Data Analysis and Statistics. All electrophysiology data were analyzed using IgorPro v6 (WaveMetrics). Curves were fit by a nonlinear least-squares method (Levenberg-Marquardt algorithm). Average values are reported as mean ± SEM, except in Fig. 4 and Table S3, which report mean ± SD. We tested significance by Student t tests or multifactorial ANOVAs, using Instat3 (GraphPad) or Statistica 9 (StatSoft), respectively.

ACKNOWLEDGMENTS. We thank Zhao-Wen Wang for plasmids encoding SLO-1(A2;B0;C1), R. Fettiplace and members of the M.B.G. and R.W.A. laboratories for comments, and wormbase.org. This work was supported by the A. P. Sloan, Mathers, and Donald D. and Delia E. Baxter Foundations, National Institutes of Health Grants NS047715 and NS061147, and Muscular Dystrophy Association Grant MDA#4206 (to M.B.G); a predoctoral Ruth L. Kirschstein Fellowship (to B.E.J); and Fellowships for Prospective Researchers from the Swiss National Science Foundation (to D.A.G. and E.S.D.-G.).

1. Pan Q, Shai O, Lee LJ, Frey BJ, Blencowe BJ (2008) Deep surveying of alternative splicing complexity in the human transcriptome by high-throughput sequencing. *Nat Genet* 40:1413–1415.
2. Wang ET, et al. (2008) Alternative isoform regulation in human tissue transcriptomes. *Nature* 456:470–476.
3. Hiller M, Huse K, Platzer M, Backofen R (2005) Creation and disruption of protein features by alternative splicing—a novel mechanism to modulate function. *Genome Biol* 6:R58.
4. Resch A, et al. (2004) Assessing the impact of alternative splicing on domain interactions in the human proteome. *J Proteome Res* 3:76–83.
5. Beisel KW, et al. (2007) Diversity of Ca2+-activated K+ channel transcripts in inner ear hair cells. *Gene* 386(1–2):11–23.
6. Fodor AA, Aldrich RW (2009) Convergent evolution of alternative splices at domain boundaries of the BK channel. *Annu Rev Physiol* 71:19–36.
7. Wang ZW, Saifee O, Nonet ML, Salkoff L (2001) SLO-1 potassium channels control quantal content of neurotransmitter release at the *C. elegans* neuromuscular junction. *Neuron* 32:867–881.
8. Knot HJ, Standen NB, Nelson MT (1998) Ryanodine receptors regulate arterial diameter and wall [Ca^{2+}] in cerebral arteries of rat via Ca^{2+}-dependent K^+ channels. *J Physiol* 508:211–221.
9. Brayden JE, Nelson MT (1992) Regulation of arterial tone by activation of calcium-dependent potassium channels. *Science* 256:532–535.
10. Brenner R, et al. (2000) Vasoregulation by the beta1 subunit of the calcium-activated potassium channel. *Nature* 407:870–876.
11. Shipston MJ, Kelly JS, Antoni FA (1996) Glucocorticoids block protein kinase A inhibition of calcium-activated potassium channels. *J Biol Chem* 271:9197–9200.
12. Lovell PV, McCobb DP (2001) Pituitary control of BK potassium channel function and intrinsic firing properties of adrenal chromaffin cells. *J Neurosci* 21:3429–3442.
13. Roberts WM, Jacobs RA, Hudspeth AJ (1990) Colocalization of ion channels involved in frequency selectivity and synaptic transmission at presynaptic active zones of hair cells. *J Neurosci* 10:3664–3684.
14. Robitaille R, Charlton MP (1992) Presynaptic calcium signals and transmitter release are modulated by calcium-activated potassium channels. *J Neurosci* 12:297–305.
15. Fettiplace R, Fuchs PA (1999) Mechanisms of hair cell tuning. *Annu Rev Physiol* 61:809–834.
16. Chen L, et al. (2005) Functionally diverse complement of large conductance calcium- and voltage-activated potassium channel (BK) alpha-subunits generated from a single site of splicing. *J Biol Chem* 280:33599–33609.

17. Saito M, Nelson C, Salkoff L, Lingle CJ (1997) A cysteine-rich domain defined by a novel exon in a slo variant in rat adrenal chromaffin cells and PC12 cells. *J Biol Chem* 272:11710–11717.
18. Shipston MJ, Duncan RR, Clark AG, Antoni FA, Tian L (1999) Molecular components of large conductance calcium-activated potassium (BK) channels in mouse pituitary corticotropes. *Mol Endocrinol* 13:1728–1737.
19. MacDonald SH, Ruth P, Knaus HG, Shipston MJ (2006) Increased large conductance calcium-activated potassium (BK) channel expression accompanied by STREX variant downregulation in the developing mouse CNS. *BMC Dev Biol* 6:37.
20. Zhu N, et al. (2005) Alternative splicing of Slo channel gene programmed by estrogen, progesterone and pregnancy. *FEBS Lett* 579:4856–4860.
21. McCartney CE, et al. (2005) A cysteine-rich motif confers hypoxia sensitivity to mammalian large conductance voltage- and Ca-activated K (BK) channel alpha-subunits. *Proc Natl Acad Sci USA* 102:17870–17876.
22. Xia XM, Zeng X, Lingle CJ (2002) Multiple regulatory sites in large-conductance calcium-activated potassium channels. *Nature* 418:880–884.
23. Schreiber M, Salkoff L (1997) A novel calcium-sensing domain in the BK channel. *Biophys J* 73:1355–1363.
24. Jiang Y, Pico A, Cadene M, Chait BT, MacKinnon R (2001) Structure of the RCK domain from the *E. coli* K^+ channel and demonstration of its presence in the human BK channel. *Neuron* 29:593–601.
25. Yuan P, Leonetti MD, Pico AR, Hsiung Y, MacKinnon R (2010) Structure of the human BK channel Ca^{2+}-activation apparatus at 3.0 A resolution. *Science* 329:182–186.
26. Wu Y, Yang Y, Ye S, Jiang Y (2010) Structure of the gating ring from the human large-conductance Ca(2+)-gated K(+) channel. *Nature* 466:393–397.
27. Wang L, Sigworth FJ (2009) Structure of the BK potassium channel in a lipid membrane from electron cryomicroscopy. *Nature* 461:292–295.
28. Jiang Y, et al. (2002) Crystal structure and mechanism of a calcium-gated potassium channel. *Nature* 417:515–522.
29. Lagrutta A, Shen KZ, North RA, Adelman JP (1994) Functional differences among alternatively spliced variants of Slowpoke, a *Drosophila* calcium-activated potassium channel. *J Biol Chem* 269:20347–20351.
30. Tian L, et al. (2001) Alternative splicing switches potassium channel sensitivity to protein phosphorylation. *J Biol Chem* 276:7717–7720.
31. Tang XD, et al. (2003) Haem can bind to and inhibit mammalian calcium-dependent Slo1 BK channels. *Nature* 425:531–535.
32. Adelman JP, et al. (1992) Calcium-activated potassium channels expressed from cloned complementary DNAs. *Neuron* 9:209–216.
33. Jones EM, Gray-Keller M, Fettiplace R (1999) The role of Ca^{2+}-activated K^+ channel splice variants in the tonotopic organization of the turtle coclea. *J Physiol* 518: 653–665.
34. Cui J, Aldrich RW (2000) Allosteric linkage between voltage and Ca(2+)-dependent activation of BK-type mslo1 K(+) channels. *Biochemistry* 39:15612–15619.
35. Chen B, et al. (2010) A novel auxiliary subunit critical to BK channel function in *Caenorhabditis elegans*. *J Neurosci* 30:16651–16661.
36. Kim H, et al. (2009) The dystrophin complex controls bk channel localization and muscle activity in *Caenorhabditis elegans*. *PLoS Genet* 5:e1000780.
37. Liu Q, Chen B, Ge Q, Wang ZW (2007) Presynaptic Ca2+/calmodulin-dependent protein kinase II modulates neurotransmitter release by activating BK channels at *Caenorhabditis elegans* neuromuscular junction. *J Neurosci* 27:10404–10413.
38. Glauser DA, Johnson BE, Aldrich RW, Goodman MB (2011) Intragenic alternative splicing coordingation is essential for *Caenorhabditis elegans slo-1* gene function. *Proc Natl Acad Sci USA* 108:20790–20795.
39. Chen L, Shipston MJ (2008) Cloning of potassium channel splice variants from tissues and cells. *Methods Mol Biol* 491:35–60.
40. Derst C, et al. (2003) The large conductance Ca^{2+}-activated potassium channel (pSlo) of the cockroach *Periplaneta americana*: Structure, localization in neurons and electrophysiology. *Eur J Neurosci* 17:1197–1212.
41. Yu JY, Upadhyaya AB, Atkinson NS (2006) Tissue-specific alternative splicing of BK channel transcripts in *Drosophila*. *Genes Brain Behav* 5:329–339.
42. Zeng XH, Xia XM, Lingle CJ (2005) Divalent cation sensitivity of BK channel activation supports the existence of three distinct binding sites. *J Gen Physiol* 125:273–286.
43. Wang B, Rothberg BS, Brenner R (2009) Mechanism of increased BK channel activation from a channel mutation that causes epilepsy. *J Gen Physiol* 133:283–294.
44. Lee JH, et al. (2009) Modulation of the conductance-voltage relationship of the BK(Ca) channel by shortening the cytosolic loop connecting two RCK domains. *Biophys J* 97:730–737.
45. Goodman MB, Lockery SR (2000) Pressure polishing: A method for re-shaping patch pipettes during fire polishing. *J Neurosci Methods* 100:13–15.
46. Pieper U, et al. (2009) MODBASE, a database of annotated comparative protein structure models and associated resources. *Nucleic Acids Res* 37(Database issue): D347–D354.